The Journal of Physical Chemistry Letters

Letter

Cite This: J. Phys. Chem. Lett. 2017, 8, 5507-5512

pubs.acs.org/JPCL

Predictive Determination of Band Gaps of Inorganic Halide Perovskites

Julia Wiktor,*[,†] Ursula Rothlisberger,[‡] and Alfredo Pasquarello[†]

[†]Chaire de Simulation à l'Echelle Atomique (CSEA), Ecole Polytechnique Fédérale de Lausanne (EPFL), CH-1015 Lausanne, Switzerland

[‡]Laboratory of Computational Chemistry and Biochemistry, Ecole Polytechnique Fédérale de Lausanne (EPFL), CH-1015 Lausanne, Switzerland

Supporting Information

ABSTRACT: We carry out first-principles calculations of band gaps of cubic inorganic perovskites belonging to the class $CsBX_3$, with B = Pb, Sn and X = Cl, Br, I. We use the quasi-particle self-consistent *GW* method with efficient vertex corrections to calculate the electronic structure of the studied materials. We demonstrate the importance of including the higher-lying core and semicore shells among the valence states. For a meaningful comparison with experimental values, we account for thermal vibrations and disorder through ab initio molecular dynamics. Additionally, we calculate the spin−orbit coupling at levels of theory of increasing accuracy and show that semilocal density functionals significantly underestimate these corrections. We show that all of these effects need to be properly included in order to obtain reliable predictions for the band gaps of halide perovskites.

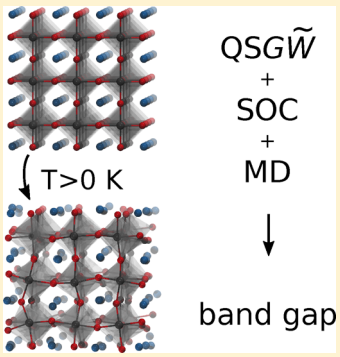

Metal−halide perovskites have attracted great attention as promising materials for high-efficiency solar cells.[1−3] The photoelectric conversion efficiencies of devices based on this class of materials have reached 22.1% in only a few years since their advent.[4] Because halide perovskites consist of abundant elements, they have the potential to combine high efficiency with low cost. Currently, extensive efforts are still being made to find compounds that could be used to produce efficient, nontoxic, and cheap solar cells.[5−8] To identify novel compounds with optimal optical properties, a modeling approach yielding accurate predictions for their band gaps is highly desirable.

In this Letter, we set out to assess the accuracy by which advanced electronic structure methods give the band gap of halide perovskites. To this end, we focus on a class of cubic inorganic perovskites given by the formula $CsBX_3$ (see Figure 1), in which B stands for Pb or Sn and X for a halide atom (Cl, Br, or I). This class of perovskites carries the advantage of a small unit cell for permitting high-level calculations and is yet representative of the larger class of organic halide perovskites as the band-edge states mainly result from the inorganic network. After setting a reference at the hybrid functional level, we mainly focus on *GW* calculations in various schemes, up to involving full self-consistency and vertex corrections in the screening. In particular, our study devotes special attention to effects associated with the inclusion of deep-lying states, thermal disorder, and spin−orbit interaction. When all of these effects are properly accounted for, the quasi-particle self-consistent *GW* scheme including efficient treatment of vertex corrections is found to give an excellent description of the experimental results.

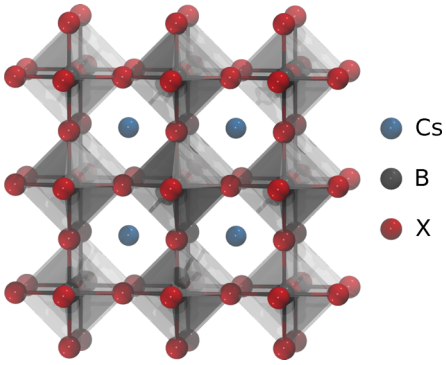

Figure 1. Representation of the crystal structure of the cubic perovskites belonging to the class $CsBX_3$, with B = Pb, Sn and X = Cl, Br, I.

Methods. The band gap calculations presented here are carried out at several levels of theory. First, we perform calculations within density functional theory (DFT) based on the semilocal Perdew−Burke−Ernzerhof (PBE) functional. Next, we turn to the hybrid functionals, proposed by Perdew, Burke, and Ernzerhof (PBE0)[9] and by Heyd, Scuseria, and Ernzerhof (HSE).[10,11] The fraction of nonlocal Fock exchange

Received: October 6, 2017
Accepted: October 27, 2017
Published: October 27, 2017

DOI: 10.1021/acs.jpclett.7b02648
J. Phys. Chem. Lett. 2017, 8, 5507−5512

is set to 25% in both of these functionals, as in the original proposals. Further, we apply the many-body perturbation theory based on Hedin's *GW* scheme.[12] We perform both one-shot G_0W_0 calculations with a PBE starting point and quasiparticle self-consistent QS$G\tilde{W}$ calculations including an efficient exchange−correlation kernel to account for vertex corrections in the screened interaction potential W.[13] The latter scheme has been shown to yield good agreement with experiment for a wide range of materials.[13] We note that the standard QS*GW* method,[14,15] which does not include a kernel for vertex corrections, systematically overestimates the values of the band gaps.[15−17] Core−valence interactions in all calculations are treated through norm-conserving pseudopotentials.[18] More details on the calculations can be found in the Supporting Information.

Halogen Semicore Electrons. First, we examine the effect of including the higher-lying core and semicore shells among the valence functions. In Table 1, we compare band gaps of $CsPbI_3$ achieved at various levels of theory, including 7 (5s and 5p), 17 (4d, 5s, and 5p), and 25 (4s, 4p, 4d, 5s, and 5p) electrons among the valence states of I (I^{7+}, I^{17+}, and I^{25+} configurations, respectively). At the PBE level, the different pseudopotentials give the same band gap. For the hybrid functionals HSE and PBE0, the band gap calculated with 17 valence electrons is larger by 0.2 eV than that achieved with only 7 valence electrons. For the I^{25+} configuration, in which the whole fourth shell is included among the valence states, the band gap achieved with the I^{7+} configuration is restored. This suggests that partial inclusion of the fourth shell leads to band gap errors. In the *GW* methods, the overestimation of the band gap due to the use of the pseudopotential with 17 valence electrons is even more prounounced. In the case of QS$G\tilde{W}$, the use of an improper pseudopotential can lead to a deviation of almost 1 eV.

Table 1. Band Gap (eV) of $CsPbI_3$, $CsPbBr_3$, and $CsPbCl_3$ Calculated at Various Levels of Theory Using Different Pseudopotential Configurations[a]

	$CsPbI_3$		
	I^{7+}	I^{17+}	I^{25+}
PBE	1.14	1.14	1.14
HSE	1.43	1.62	1.45
PBE0	2.04	2.26	2.08
G_0W_0	1.82	2.29	1.89
QS$G\tilde{W}$	2.03	3.05	2.24
	$CsPbBr_3$		
	Br^{7+}	Br^{17+}	Br^{25+}
PBE	1.54	1.54	1.54
G_0W_0	2.55	3.22	2.56
	$CsPbCl_3$		
	Cl^{5+}		Cl^{15+}
PBE	1.94		1.93
G_0W_0	3.36		2.93

[a]Calculations are performed at the experimental lattice constant.

The importance of the number of valence electrons in *GW* calculations of halide perovskites has already been pointed out. Filip and Giustino[19] noticed that including 17 valence electrons in the pseudopotential of I increases the band gap in the case of $CH_3NH_3PbI_3$. They adopted this pseudopotential in their QS*GW* calculations of $CH_3NH_3PbI_3$ and $CsPbI_3$. In the case of $CH_3NH_3PbI_3$, it was later observed by Scherpelz et al.[20] that the I^{17+} pseudopotential yields band gaps significantly larger than those obtained with 7 or 25 valence electrons due to the incomplete treatment of the semicore electron shell. This observation is consistent with the present calculations for $CsPbI_3$. Interestingly, in both cited studies, it was noted that the best agreement with experiment is achieved with the I^{17+} pseudopotential. At variance, we argue in this work that the observed agreement was due to error cancellation, as will become clear from the following.

We also study the influence of the pseudopotential configuration on the calculated band gap in the case of Br and Cl. The results are given in Table 1. For Br, we notice that, as in the case of I, the configuration with 17 valence electrons leads to overestimation of the band gap at the *GW* level. In the case of Cl, we similarly observe that the Cl^{15+} pseudopotential configuration is required to obtain converged results at the *GW* level of theory. On the basis of the above tests, we use I^{25+}, Br^{25+}, and Cl^{15+} pseudopotential configurations in the following band gap calculations.

In Table 2, we compare the band gaps of the considered inorganic halide perovskites achieved with PBE, HSE, PBE0, G_0W_0, and QS$G\tilde{W}$. For all of the considered halide perovskites, the HSE hybrid functional opens the PBE band gap by only 0.26−0.45 eV. The PBE0 hybrid functional and the one-shot G_0W_0 method lead to slightly larger band gaps. However, none of these methods succeeds in reproducing the larger band gaps achieved with the more accurate QS$G\tilde{W}$ technique.

Table 2. Band Gaps (eV) of Inorganic Halide Perovskites in the Cubic Phase, Calculated at Various Levels of Theory[a]

	PBE	HSE	PBE0	G_0W_0	QS$G\tilde{W}$
$CsPbI_3$	1.14	1.45	2.08	1.89	2.24
$CsPbBr_3$	1.54	1.95	2.61	2.56	3.15
$CsPbCl_3$	1.93	2.38	3.07	2.93	3.66
$CsSnI_3$	0.33	0.59	1.17	0.82	1.21
$CsSnBr_3$	0.41	0.74	1.34	1.02	1.66
$CsSnCl_3$	0.80	1.17	1.81	1.40	2.22

[a]Calculations are performed at the experimental lattice constant.

Thermal Effects. To make a meaningful comparison between band gaps calculated at 0 K and experimental data measured at finite temperature, the effects of disorder and atomic vibrations have to be taken into account. To account for the thermal disorder, we perform 10 ps long ab initio Born−Oppenheimer molecular dynamics (MD) simulations in the *NpT* ensemble at a pressure of 1 atm.[21]

In the simulations, we allow for the change of supercell volume while keeping its cubic shape. The temperature is set to the value at which the experimental lattice parameters were measured (see Table 3). In the MD runs, we use the revised Vydrov and Van Voorhis (rVV10) nonlocal density functional[22,23] to improve the description of the interatomic interactions. We choose this particular functional because it yields lattice parameters in very good agreement with calculations at the PBE0 level of theory for the present set of materials (see Table S1 in the Supporting Information). Moreover, we study the effect of the electronic structure method on the band gap renormalization by performing additional calculations within the PBE0 functional on 50 snapshots chosen from the MD trajectory. From the MD simulations, we only want to extract the effect of atomic

DOI: 10.1021/acs.jpclett.7b02648
J. Phys. Chem. Lett. 2017, 8, 5507−5512

Table 3. Band Gap Opening Due to the Finite Temperature T, Calculated with rVV10 and PBE0 Functionals on Configurations Achieved through MD Simulations[a]

	Δ_T^{rVV10} (eV)	Δ_T^{PBE0} (eV)	T (K)
$CsPbI_3$	0.47	0.74	300
$CsPbBr_3$	0.39	0.51	403
$CsPbCl_3$	0.50	0.63	320
$CsSnI_3$	0.64	0.78	425
$CsSnBr_3$	0.64	0.77	300
$CsSnCl_3$	0.62	0.73	390

[a] T corresponds to the temperature at which the the cubic phase of a given material is stable or has been stabilized.

vibrations. This is because the $QSG\tilde{W}$ band gaps are calculated at the experimental lattice constant observed at finite temperature, which already includes the thermal expansion. Therefore, we calculate the renormalization Δ_{gap}^T as

$$\Delta_{gap}^T = E_{gap}^{MD}(a_{MD}) - E_{gap}^{0K}(a_{MD}) \quad (1)$$

where $E_{gap}^{MD}(a_{MD})$ is the time-averaged band gap resulting from the MD simulation at finite temperature and $E_{gap}^{0K}(a_{MD})$ is the band gap calculated at 0 K at the equilibrium lattice constant a_{MD} resulting from the MD. We note that the differences between the equilibrium lattice parameters at 0 K and at finite temperature are found to be rather small. They amount to about 0.01 Å for the lead-based compounds and to 0.04−0.07 Å for the tin-based ones. The small thermal expansion of the cubic halide perovskites is consistent with a previous study on $CsSnI_3$.[24]

The band gap renormalization due to temperature is shown in Table 3. We observe that for all considered materials, finite temperature leads to a strong opening of the band gap, which is consistent with previous studies.[25−27] At the semilocal level, this effect increases the gap by 0.39 to 0.64 eV, depending on the material. With the PBE0 functional, we find that the temperature effects lead to even larger band gap openings, ranging between 0.51 and 0.80 eV. The increase of the band gap due to finite temperature suggests that this effect cannot be neglected when comparing calculated band gaps with experiment. The present findings are consistent with a recent study on the temperature dependence of the energy levels in halide perovskites based on electron−phonon calculations.[26] Therein, Saidi et al. found a band gap renormalization of about 0.4 eV for $CsPbI_3$ at 300 K. This result, achieved with semilocal functionals, is in very good agreement with the value of 0.47 eV calculated here with the rVV10 functional.

To understand better the origin of such an important temperature effect on the band gap, we analyze the structure of the considered materials at finite temperature. It has been shown that the band gap of halide perovskites strongly correlates with the metal−halide−metal bond angle[28] and the metal−halide bond length.[29] Therefore, we focus on these two parameters and provide their average values at finite temperature in Table 4. We observe an average bond angle of about 168° for all of the studied materials. The average metal−halide bond length at finite temperature is by 0.05−0.1 Å larger than that at 0 K. Both of these effects explain qualitatively the band gap opening observed in the present study. Our MD results are in agreement with a recent study of Yang et al.,[27] who observed double-well potential energy surfaces in cubic halide perovskites leading to spontaneous octahedral tilting. The local breaking of the cubic symmetry and the octahedral tilting observed during

Table 4. Average Metal−Halide−Metal Bond Angle ϕ^T and Average Metal−Halide Bond Length d_{M-H}^T As Found in the MD Simulations at the Finite Temperature T[a]

	ϕ^{0K} (deg)	ϕ^T (deg)	d_{M-H}^{0K} (Å)	d_{M-H}^T (Å)
$CsPbI_3$	180	168	3.16	3.27
$CsPbBr_3$	180	168	2.97	3.06
$CsPbCl_3$	180	168	2.84	2.91
$CsSnI_3$	180	167	3.16	3.24
$CsSnBr_3$	180	169	2.95	3.02
$CsSnCl_3$	180	168	2.82	2.87

[a] See Table 3. The values are compared with their counterparts at 0 K, obtained by relaxing the system at the equilibrium lattice constant resulting from the MD.

the MD simulations are shown in Figure 2 in the case of $CsSnBr_3$. For the other materials, similar effects are observed.

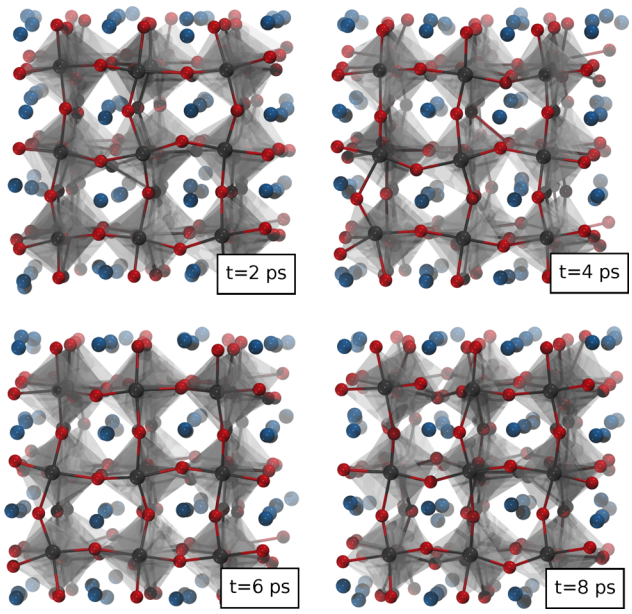

Figure 2. Snapshots from the ab initio MD run of $CsSnBr_3$ at 300 K.

We note that the band gap renormalization due to finite temperature is particularly large in the case of cubic inorganic halide perovskites. This is due to the fact that the difference in band gap is calculated between a disordered structure at finite temperature and a highly symmetric structure at 0 K. The perfect cubic arrangement results in a maximum (antibonding) overlap between the p orbitals of the halide and the s orbitals of the metal that make up the top of the valence band. Therefore, the deviations from the perfect structure due to disorder reduce this overlap significantly and lead to stabilization of the top of the valence band. We expect the effect of temperature to be smaller for other phases of the studied materials and for perovskites containing organic molecules, in which some disorder is already present at 0 K.

Spin−Orbit Coupling. The band gaps of the halide perovskites under investigation in this work are strongly affected by spin−orbit coupling (SOC). We first examine the influence of the level of theory used for the evaluation of SOC effects. In Table 5, we compare SOC corrections as calculated at the semilocal density functional and G_0W_0 levels of theory. We observe that for $CsPbI_3$, $CsPbCl_3$, and $CsPbBr_3$, the PBE functional underestimates the spin−orbit effect on the band gap by

DOI: 10.1021/acs.jpclett.7b02648
J. Phys. Chem. Lett. 2017, 8, 5507−5512

Table 5. Band Gap Corrections Due to SOC (eV), Calculated at the Semilocal Density Functional and G_0W_0 Levels of Theory, at 0 K and at Finite Temperature T Given in Table 3[a]

	Δ_{SOC}^{PBE} (eV)		$\Delta_{SOC}^{G_0W_0}$ (eV)	
	0 K	T	0 K	T
$CsPbI_3$	−1.25	−0.96	−1.51	−1.22
$CsPbBr_3$	−1.23	−0.89	−1.62	−1.28
$CsPbCl_3$	−1.23	−0.97	−1.60	−1.34
$CsSnI_3$	−0.39	−0.28	−0.51	−0.40
$CsSnBr_3$	−0.36	−0.25	−0.45	−0.34
$CsSnCl_3$	−0.35	−0.24	−0.46	−0.35

[a]In the case of G_0W_0, we apply the PBE reduction of the SOC correction due to thermal effects.

about 0.3 eV, on average. For the tin-based compounds, we find that the underestimation reduces to about 0.1 eV. These results highlight the necessity of treating the SOC at higher levels of theory in the case of halide perovskites. We note that the difference between SOC corrections to the band gap calculated at the semilocal density functional and GW levels has already been pointed out for $CH_3NH_3PbI_3$.[19,20,30]

Because our goal is to compare the calculated band gaps with experimental values measured at finite temperature, we next study the effect of thermal disorder on the SOC. This is done by calculating band gaps with and without SOC for structures taken from the MD trajectory. At the PBE level, we observe that the band gap closing due to the SOC is smaller at finite temperatures (see Table 5). Because the numerical cost of G_0W_0 calculations for supercells is prohibitive, we apply the PBE reduction of the SOC correction due to thermal effects without change to the G_0W_0 level of theory.

Comparison with Experiments. Once the effects of SOC and thermal renormalization are taken into account, the calculated band gaps can be compared with experiment. In Table 6, we give our best estimates of the band gaps, calculated as

$$E_{gap}^{theory} = E_{gap}^{QSG\tilde{W}} + \Delta_T^{PBE0} + \Delta_{SOC}^{G_0W_0} \quad (2)$$

where $E_{gap}^{QSG\tilde{W}}$ is the band gap calculated with $QSG\tilde{W}$ at 0 K, Δ_T^{PBE0} is the effect of temperature calculated using the PBE0 functional, and $\Delta_{SOC}^{G_0W_0}$ is the estimated G_0W_0 correction due to SOC at finite temperature. We estimate the errors on the thermal and SOC corrections due to the combination of different levels of theory (see the Supporting Information) to be lower than 0.03 eV. The calculated band gaps are compared with the experimental optical band gaps when available (cf. Table 6). We observe very good agreement between the calculated and measured band gaps. In the comparison, we have neglected the exciton binding energies, which are expected to be on the order of tens to 100 meVs.[28,31−35] We note that because our theoretical estimates are generally slightly larger than the experimental values, including the excitonic effects would lead to an even better agreement.

Table 6. Best Theoretical Estimates Achieved in This Work for the Band Gap of a Series of Inorganic Halide Perovskites, Compared with Experimental Optical Band Gaps along with the $QSG\tilde{W}$ Results at 0 K and the Corrections to the Band Gap Due to Finite Temperature and SOC

	$E_{gap}^{QSG\tilde{W}}$	Δ_T^{PBE0}	$\Delta_{SOC}^{G_0W_0}$	E_{gap}^{theory} (eV)	E_{gap}^{expt} (eV)
$CsPbI_3$	2.24	0.74	−1.22	1.76	1.67,[a] 1.73[b]
$CsPbBr_3$	3.15	0.51	−1.28	2.38	2.36[c]
$CsPbCl_3$	3.66	0.63	−1.34	2.95	2.85[d]
$CsSnI_3$	1.21	0.78	−0.40	1.57	
$CsSnBr_3$	1.66	0.77	−0.34	2.09	
$CsSnCl_3$	2.22	0.73	−0.35	2.60	∼2.6[e]

[a]Experimental values come from ref 36. [b]Experimental values come from ref 37. [c]Experimental values come from ref 38. [d]Experimental values come from ref 39. [e]Experimental values come from ref 40.

We note that good agreement with experiment was generally observed in previous computational studies on band gaps of halide perovskites. However, the important thermal effects had not been accounted for in these calculations. Therefore, the apparent good agreement with experiment observed in most of the previous GW calculations for halide perovskites should be assigned to fortuitous error cancellation. In the case of halide perovskites, there are multiple sources of errors, which could stem from, for example, neglecting the thermal effects, using incomplete valence manifolds in the pseudopotentials,[19,41] omitting vertex corrections in the $QSGW$ calculations,[32] or performing calculations at overestimated DFT volumes.[42] We emphasize that the agreement between the calculated and experimental values can only be achieved when an accurate electronic structure method (here $QSG\tilde{W}$) is applied and all of the significant effects (SOC and thermal disorder) are correctly accounted for.

In summary, we performed electronic structure calculations for a series of cubic inorganic halide perovskites at various levels of theory. We studied the effect of including the higher-lying core and semicore shells among the valence states and observed that the use of an incomplete valence manifold in the pseudopotential of the halogen atom can lead to important errors in the band gap calculations. Moreover, we compared the performance of various levels of theory in calculating the band gaps. It was shown that the quasi-particle self-consistent GW method, in which vertex corrections are accounted for, gives a reliable scheme for calculating the electronic structure of this class of materials. To compare with band gaps measured at finite temperature, we calculated the band gap renormalization due to the thermal motion of the atoms. This was achieved by means of ab initio MD simulations. Finally, we addressed the influence of the SOC on the band gap. It is shown that the evaluation of this effect requires consideration of an appropriate level of theory and of the thermal disorder. The present study shows that a meaningful comparison with experiment can only be made after proper treatment of the aforementioned effects, which are all found to be sizable. In turn, their consideration leads to theoretical band gaps in very good agreement with experiment.

■ ASSOCIATED CONTENT

Supporting Information

The Supporting Information is available free of charge on the ACS Publications website at DOI: 10.1021/acs.jpclett.7b02648.

Computational details on the GW, molecular dynamics, and spin−orbit coupling calculations (PDF)

■ AUTHOR INFORMATION

Corresponding Author

*E-mail: julia.wiktor@epfl.ch

DOI: 10.1021/acs.jpclett.7b02648
J. Phys. Chem. Lett. 2017, 8, 5507−5512

ORCID

Julia Wiktor: 0000-0003-3395-1104
Alfredo Pasquarello: 0000-0002-9142-2799

Notes

The authors declare no competing financial interest.

■ ACKNOWLEDGMENTS

The authors acknowledge O. Syzgantseva for useful discussions. This work has been realized in relation to the National Center of Competence in Research (NCCR) "Materials' Revolution: Computational Design and Discovery of Novel Materials (MARVEL)" of the SNSF. We used computational resources of the Swiss National Supercomputing Centre and of the Ecole Polytechnique Fédérale de Lausanne.

■ REFERENCES

(1) Kojima, A.; Teshima, K.; Shirai, Y.; Miyasaka, T. Organometal Halide Perovskites As Visible-Light Sensitizers for Photovoltaic Cells. *J. Am. Chem. Soc.* **2009**, *131*, 6050−6051.

(2) Kim, H.-S.; Lee, C.-R.; Im, J.-H.; Lee, K.-B.; Moehl, T.; Marchioro, A.; Moon, S.-J.; Humphry-Baker, R.; Yum, J.-H.; Moser, J. E.; et al. Lead Iodide Perovskite Sensitized All-Solid-State Submicron Thin Film Mesoscopic Solar Cell with Efficiency Exceeding 9%. *Sci. Rep.* **2012**, *2*, 591.

(3) Hodes, G. Perovskite-Based Solar Cells. *Science* **2013**, *342*, 317−318.

(4) Yang, W. S.; Park, B.-W.; Jung, E. H.; Jeon, N. J.; Kim, Y. C.; Lee, D. U.; Shin, S. S.; Seo, J.; Kim, E. K.; Noh, J. H.; et al. Iodide Management in Formamidinium-Lead-Halide-Based Perovskite Layers for Efficient Solar Cells. *Science* **2017**, *356*, 1376−1379.

(5) Castelli, I. E.; García-Lastra, J. M.; Thygesen, K. S.; Jacobsen, K. W. Bandgap Calculations and Trends of Organometal Halide Perovskites. *APL Mater.* **2014**, *2*, 081514.

(6) Filip, M. R.; Giustino, F. Computational Screening of Homovalent Lead Substitution in Organic-Inorganic Halide Perovskites. *J. Phys. Chem. C* **2016**, *120*, 166−173.

(7) Körbel, S.; Marques, M. A.; Botti, S. Stability and Electronic Properties of New Inorganic Perovskites from High-Throughput Ab Initio Calculations. *J. Mater. Chem. C* **2016**, *4*, 3157−3167.

(8) Jain, A.; Voznyy, O.; Sargent, E. H. High-Throughput Screening of Lead-Free Perovskite-like Materials for Optoelectronic Applications. *J. Phys. Chem. C* **2017**, *121*, 7183−7187.

(9) Perdew, J. P.; Ernzerhof, M.; Burke, K. Rationale for Mixing Exact Exchange with Density Functional Approximations. *J. Chem. Phys.* **1996**, *105*, 9982−9985.

(10) Heyd, J.; Scuseria, G. E.; Ernzerhof, M. Hybrid Functionals Based on a Screened Coulomb Potential. *J. Chem. Phys.* **2003**, *118*, 8207−8215.

(11) Heyd, J.; Scuseria, G. E.; Ernzerhof, M. Erratum: "Hybrid Functionals Based on a Screened Coulomb Potential" [J. Chem. Phys. 118, 8207 (2003)]. *J. Chem. Phys.* **2006**, *124*, 219906.

(12) Hedin, L. New Method for Calculating the One-Particle Green's Function with Application to the Electron-Gas Problem. *Phys. Rev.* **1965**, *139*, A796.

(13) Chen, W.; Pasquarello, A. Accurate Band Gaps of Extended Systems via Efficient Vertex Corrections in *GW*. *Phys. Rev. B: Condens. Matter Mater. Phys.* **2015**, *92*, 041115.

(14) Faleev, S. V.; Van Schilfgaarde, M.; Kotani, T. All-Electron Self-Consistent *GW* Approximation: Application to Si, MnO, and NiO. *Phys. Rev. Lett.* **2004**, *93*, 126406.

(15) van Schilfgaarde, M.; Kotani, T.; Faleev, S. Quasiparticle Self-Consistent *GW* Theory. *Phys. Rev. Lett.* **2006**, *96*, 226402.

(16) Shishkin, M.; Marsman, M.; Kresse, G. Accurate Quasiparticle Spectra from Self-Consistent *GW* Calculations with Vertex Corrections. *Phys. Rev. Lett.* **2007**, *99*, 246403.

(17) Chen, W.; Pasquarello, A. Band-Edge Positions in *GW*: Effects of Starting Point and Self-Consistency. *Phys. Rev. B: Condens. Matter Mater. Phys.* **2014**, *90*, 165133.

(18) Hamann, D. Optimized Norm-Conserving Vanderbilt Pseudopotentials. *Phys. Rev. B: Condens. Matter Mater. Phys.* **2013**, *88*, 085117.

(19) Filip, M. R.; Giustino, F. *GW* Quasiparticle Band Gap of the Hybrid Organic-Inorganic Perovskite $CH_3NH_3PbI_3$: Effect of Spin-Orbit Interaction, Semicore Electrons, and Self-Consistency. *Phys. Rev. B: Condens. Matter Mater. Phys.* **2014**, *90*, 245145.

(20) Scherpelz, P.; Govoni, M.; Hamada, I.; Galli, G. Implementation and Validation of Fully Relativistic *GW* Calculations: Spin-Orbit Coupling in Molecules, Nanocrystals, and Solids. *J. Chem. Theory Comput.* **2016**, *12*, 3523−3544.

(21) Martyna, G. J.; Tuckerman, M. E.; Tobias, D. J.; Klein, M. L. Explicit Reversible Integrators for Extended Systems Dynamics. *Mol. Phys.* **1996**, *87*, 1117−1157.

(22) Vydrov, O. A.; Van Voorhis, T. Nonlocal Van Der Waals Density Functional: The Simpler the Better. *J. Chem. Phys.* **2010**, *133*, 244103.

(23) Sabatini, R.; Gorni, T.; de Gironcoli, S. Nonlocal Van der Waals Density Functional Made Simple and Efficient. *Phys. Rev. B: Condens. Matter Mater. Phys.* **2013**, *87*, 041108.

(24) Da Silva, E. L.; Skelton, J. M.; Parker, S. C.; Walsh, A. Phase Stability and Transformations in the Halide Perovskite $CsSnI_3$. *Phys. Rev. B: Condens. Matter Mater. Phys.* **2015**, *91*, 144107.

(25) Patrick, C. E.; Jacobsen, K. W.; Thygesen, K. S. Anharmonic Stabilization and Band Gap Renormalization in the Perovskite $CsSnI_3$. *Phys. Rev. B: Condens. Matter Mater. Phys.* **2015**, *92*, 201205.

(26) Saidi, W. A.; Poncé, S.; Monserrat, B. Temperature Dependence of the Energy Levels of Methylammonium Lead Iodide Perovskite from First Principles. *J. Phys. Chem. Lett.* **2016**, *7*, 5247−5252.

(27) Yang, R. X.; Skelton, J. M.; da Silva, L.; Frost, J. M.; Walsh, A. Spontaneous Octahedral Tilting in the Cubic Inorganic Caesium Halide Perovskites $CsSnX_3$ and $CsPbX_3$ (X= F, Cl, Br, I). *J. Phys. Chem. Lett.* **2017**, *8*, 4720−4726.

(28) Filip, M. R.; Eperon, G. E.; Snaith, H. J.; Giustino, F. Steric Engineering of Metal-Halide Perovskites with Tunable Optical Band Gaps. *Nat. Commun.* **2014**, *5*, 5757.

(29) Knutson, J. L.; Martin, J. D.; Mitzi, D. B. Tuning the Band Gap in Hybrid Tin Iodide Perovskite Semiconductors Using Structural Templating. *Inorg. Chem.* **2005**, *44*, 4699−4705.

(30) Brivio, F.; Butler, K. T.; Walsh, A.; van Schilfgaarde, M. Relativistic Quasiparticle Self-Consistent Electronic Structure of Hybrid Halide Perovskite Photovoltaic Absorbers. *Phys. Rev. B: Condens. Matter Mater. Phys.* **2014**, *89*, 155204.

(31) Chen, Z.; Yu, C.; Shum, K.; Wang, J. J.; Pfenninger, W.; Vockic, N.; Midgley, J.; Kenney, J. T. Photoluminescence Study of Polycrystalline $CsSnI_3$ Thin Films: Determination of Exciton Binding Energy. *J. Lumin.* **2012**, *132*, 345−349.

(32) Huang, L.-Y.; Lambrecht, W. R. Electronic Band Structure, Phonons, and Exciton Binding Energies of Halide Perovskites $CsSnCl_3$, $CsSnBr_3$, and $CsSnI_3$. *Phys. Rev. B: Condens. Matter Mater. Phys.* **2013**, *88*, 165203.

(33) Miyata, A.; Mitioglu, A.; Plochocka, P.; Portugall, O.; Wang, J. T.-W.; Stranks, S. D.; Snaith, H. J.; Nicholas, R. J. Direct Measurement of the Exciton Binding Energy and Effective Masses for Charge Carriers in Organic-Inorganic Tri-Halide Perovskites. *Nat. Phys.* **2015**, *11*, 582−587.

(34) Yamada, Y.; Nakamura, T.; Endo, M.; Wakamiya, A.; Kanemitsu, Y. Photoelectronic Responses in Solution-Processed Perovskite $CH_3NH_3PbI_3$ Solar Cells Studied by Photoluminescence and Photoabsorption Spectroscopy. *IEEE J. Photovolt.* **2015**, *5*, 401−405.

(35) Bokdam, M.; Sander, T.; Stroppa, A.; Picozzi, S.; Sarma, D.; Franchini, C.; Kresse, G. Role of Polar Phonons in the Photo Excited State of Metal Halide Perovskites. *Sci. Rep.* **2016**, DOI: 10.1038/srep28618.

(36) Stoumpos, C. C.; Malliakas, C. D.; Kanatzidis, M. G. Semiconducting Tin and Lead Iodide Perovskites with Organic

DOI: 10.1021/acs.jpclett.7b02648
J. Phys. Chem. Lett. 2017, 8, 5507−5512

Cations: Phase Transitions, High Mobilities, and Near-Infrared Photoluminescent Properties. *Inorg. Chem.* **2013**, *52*, 9019−9038.
(37) Eperon, G. E.; Stranks, S. D.; Menelaou, C.; Johnston, M. B.; Herz, L. M.; Snaith, H. J. Formamidinium Lead Trihalide: A Broadly Tunable Perovskite for Efficient Planar Heterojunction Solar Cells. *Energy Environ. Sci.* **2014**, *7*, 982−988.
(38) Hoffman, J. B.; Schleper, A. L.; Kamat, P. V. Transformation of Sintered CsPbBr3 Nanocrystals to Cubic $CsPbI_3$ and Gradient $CsPbBr_xI_{3-x}$ Through Halide Exchange. *J. Am. Chem. Soc.* **2016**, *138*, 8603−8611.
(39) Sebastian, M.; Peters, J.; Stoumpos, C.; Im, J.; Kostina, S.; Liu, Z.; Kanatzidis, M.; Freeman, A.; Wessels, B. Excitonic Emissions and Above-Band-Gap Luminescence in the Single-Crystal Perovskite Semiconductors $CsPbBr_3$ and $CsPbCl_3$. *Phys. Rev. B: Condens. Matter Mater. Phys.* **2015**, *92*, 235210.
(40) Peedikakkandy, L.; Bhargava, P. Composition Dependent Optical, Structural and Photoluminescence Characteristics of Cesium Tin Halide Perovskites. *RSC Adv.* **2016**, *6*, 19857−19860.
(41) Filip, M. R.; Verdi, C.; Giustino, F. *GW* Band Structures and Carrier Effective Masses of $CH_3NH_3PbI_3$ and Hypothetical Perovskites of the Type $APbI_3$: A= NH_4, PH_4, AsH_4, and SbH_4. *J. Phys. Chem. C* **2015**, *119*, 25209−25219.
(42) Umari, P.; Mosconi, E.; De Angelis, F. Relativistic *GW* Calculations on $CH_3NH_3PbI_3$ and $CH_3NH_3SnI_3$ Perovskites for Solar Cell Applications. *Sci. Rep.* **2015**, *4*, 4467.

DOI: 10.1021/acs.jpclett.7b02648
J. Phys. Chem. Lett. 2017, 8, 5507−5512